Ultrasonics 122 (2022) 106689

Contents lists available at ScienceDirect

Ultrasonics

journal homepage: www.elsevier.com/locate/ultras

Unsupervised deep learning based approach to temperature monitoring in focused ultrasound treatment

Michal Byra *, Ziemowit Klimonda, Eleonora Kruglenko, Barbara Gambin

Institute of Fundamental Technological Research, Polish Academy of Sciences, Warsaw, Poland

ARTICLE INFO

Keywords:
Temperature monitoring
High intensity ultrasound
Deep learning
Transfer learning
Ultrasound imaging

ABSTRACT

Temperature monitoring in ultrasound (US) imaging is important for various medical treatments, such as high-intensity focused US (HIFU) therapy or hyperthermia. In this work, we present a deep learning based approach to temperature monitoring based on radio-frequency (RF) US data. We used Siamese neural networks in an unsupervised way to spatially compare RF data collected at different time points of the heating process. The Siamese model consisted of two identical networks initially trained on a large set of simulated RF data to assess tissue backscattering properties. To illustrate our approach, we experimented with a tissue-mimicking phantom and an *ex-vivo* tissue sample, which were both heated with a HIFU transducer. During the experiments, we collected RF data with a regular US scanner. To determine spatiotemporal variations in temperature distribution within the samples, we extracted small 2D patches of RF data and compared them with the Siamese network. Our method achieved good performance in determining the spatiotemporal distribution of temperature during heating. Compared with the temperature monitoring based on the change in radio-frequency signal backscattered energy parameter, our method provided more smooth spatial parametric maps and did not generate ripple artifacts. The proposed approach, when fully developed, might be used for US based temperature monitoring of tissues.

1. Introduction

Accurate ultrasound (US) based temperature monitoring can be useful for various medical treatments. Mild hyperthermia requires to maintain tissue temperature between 39° and 42° to induce physiological changes beneficial to patient health [1]. High intensity focused US (HIFU) is used to locally heat tissue to induce necrosis and is commonly applied for cancer treatment [2]. Various methods have been proposed to help monitor spatiotemporal changes of tissue temperature in US [3]. Temperature changes are usually not clearly visible in regular B-mode US images and therefore quantitative US (QUS) methods have been investigated to improve temperature imaging contrast. QUS techniques have been derived from various tissue physical models and utilize radio-frequency (RF) data (data before US image reconstruction) to determine parameters related to various physical properties of tissues [4]. RF data contain tissue related information that is not present in regular B-mode US images due to lossy US image reconstruction. QUS methods include estimation of backscatter and attenuation coefficients, as well as assessment of tissue micro-structure with various statistical models, for example the Nakagami distribution [5]. In the case of the temperature monitoring, change in RF signal backscattered energy (CBE) has been utilized with good results in several studies [6–8]. The aim of the CBE technique is to assess the temporal change of local backscattered echo reflectively, which results from the modification of acoustic impedance due to the heating of the tissue. Similarly, the Nakagami and Homodyned K distributions have been applied to assess the change of tissue micro-structure during the heating [9–12]. Other quantitative methods for the temperature monitoring in US include thermal strain imaging and tissue stiffness assessment [13–15].

Deep learning (DL) methods have achieved remarkable success in computer vision and medical image analysis [16,17]. These data driven machine learning techniques can automatically process and analyze input data to provide the required output, such as a classification decision. DL techniques for temperature monitoring have been proposed in several papers [18–21]. Zhang et al. developed a convolutional neural network (CNN) for detection and monitoring of thermal lesions induced by microwave ablation. Authors collected and annotated a large dataset of RF data matrices to train the neural network in a supervised manner [21]. Kim et al. utilized time of flight data collected with an US transducer to detect the change in sound velocity during thermal ablation [18]. Authors used numerical simulations mimicking their experiment to generate data and train a temperature monitoring neural network. Moreover, Chen et al. and Kim et al. developed neural

* Corresponding author.
E-mail address: mbyra@ippt.pan.pl (M. Byra).

https://doi.org/10.1016/j.ultras.2022.106689
Received 14 April 2021; Received in revised form 25 November 2021; Accepted 15 January 2022
Available online 1 February 2022

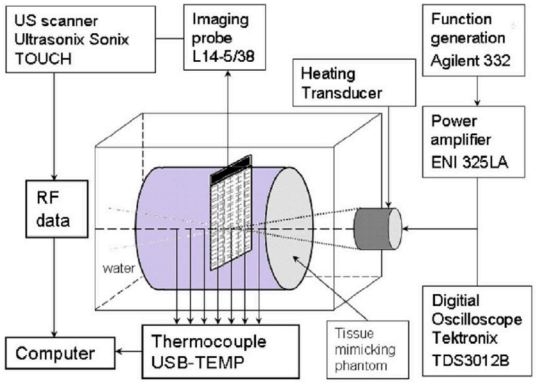

Fig. 1. Scheme of the experimental setup used in our study for the heating of the samples.

networks utilizing time of flight information for temperature monitoring in HIFU [19,20]. It is usually time consuming and expensive to conduct multiple experiments and collect large volumes of RF data that would enable supervised training of deep networks for temperature monitoring. To address this problem, in this study we propose an unsupervised DL based approach to temperature monitoring. The contributions of our work are two-fold. First, we present a unique approach to network pre-training. We numerically generate large volumes of RF data characterized by different scattering properties and use these data to develop a generic CNN for scatterer density prediction. Second, we utilize the developed CNN to perform temperature monitoring in US. A Siamese model consisting of two identical CNNs pre-trained to predict scatterer density is applied to compare RF data from the pre-heating to heating/cooling stages. In this case, we use the network to compare small 2D patches of RF data corresponding to the same spatial location, but different time points. Based on the similarity between the patches we generate parametric maps illustrating spatiotemporal distributions of tissue temperate. In computer vision, Siamese neural networks have been applied to face recognition or object tracking [22,23]. Siamese models utilize twin networks that work in a tandem to assess similarity between two separate inputs. This way it is possible to determine if the input images present the same object. In our work, we use Siamese models in a similar fashion to assess the impact of temperature variations on the RF data.

This paper is organized in the following way. First, we describe the experimental setup used to simultaneously collect RF data and heat samples with a HIFU transducer. Second, we present how we simulated large volumes of RF data and how these data were used to pre-train a CNN for scatterer density prediction. Next, we describe the proposed approach to temperature monitoring based on Siamese networks. Finally, we present and discuss the results.

2. Materials and methods

2.1. Experimental setup

Our experimental setup is presented in Fig. 1. We used a tissue-mimicking phantom and an *ex-vivo* tissue sample for the experiments. Both samples had cylindrical shape and were placed in a tank filled with degassed distilled water. Phantom was made out of water, oil and agar powder, and was filled with glass micro-particles (model 59200-U, Supelco, Bellefonte, PA, USA, diameter 75 ±5 μm) to imitate tissue microstructures [24]. The density of the glass micro-particles was equal to 16 per mm^3. Fresh pork loin bought at a local butchery shop was used to prepare the sample for the experiment. The tissue sample was degassed before inclusion into the experimental setup. HIFU transducer (Meggitt, Kvistgaard, Denmark, central frequency 2.2 MHz, diameter 44 mm and 44.5 mm focal length) was used for the heating. The average power of the focused US beam was equal to 6 W, and was determined experimentally as the power required to increase the temperature within the samples above 50 °C. The focal zone was set at a depth approximately corresponding to the center of each sample. Our experimental setup also included a pulse generator (Agilent 332, Colorado Springs USA), amplifier (ENI 325LA, Rochester NY, USA), and an oscilloscope (Tektronix TDS3012B). The samples were heated with US pulses generated by the HIFU transducer. Spatiotemporal temperature distributions were recorded along the heating beam axis with six thermocouples and a USB-TEMP module (Measurement Computing, Norton, USA). The heating/cooling stages lasted for 600 s. Thermocouples spanned the heating region, distance between the adjacent thermocouples was equal to 5 mm. Ultrasonix research US scanner (Ultrasonix, Canada) was used to collect RF data every 6 s during the heating and cooling of the samples. Linear imaging probe L14-5/38 was located above the focal spot of the HIFU transducer. Thermocouple was positioned close to the focal spot but was not visible in the imaging plane. Moreover, the imaging plane was transverse to the heating beam axis (Fig. 1). RF signal sampling rate was equal to 40 MHz. Center RF signal frequency determined using Fourier transform was equal to around 5 MHz. The HIFU pulse generator and the US scanner were synchronized to omit possible adverse interference between the imaging and heating US pulses.

2.2. Field II simulations

According to the review paper of Lewis et al., the tissue scatterer density is among the more sensitive QUS parameters to temperature variations [3]. Inspired by these findings, we generated RF data based on numerical phantoms presenting different concentrations of scatterers. Numerical simulations were performed in the Field II software, which is widely used for the simulation of US fields [25,26]. Simulations imitated the imaging setup used for the HIFU experiment. The characteristics of the simulated transducer were similar to the L14/5 linear probe, with imaging frequency of 5 MHz and pitch of 0.3 mm. Numerical phantoms consisted of point scatterers uniformly distributed in a 20 mm × 20 mm × 1 mm cuboid. Amplitudes of the scatterers and phantom attenuation coefficient were set to 1 and 0.5 dB/(MHz cm), respectively. Density of the scatterers uniformly ranged between 3.5 and 70 n/mm^3 with a step of around 3.6 n/mm^3 (20 steps). These values were selected experimentally to span a large range of different scattering conditions and include the scatterer density of the tissue-mimicking phantom. Plane wave imaging technique was applied to generate RF data. This way, the generated data were not affected by the position of the focal zone, as would be in the case of the standard beamforming [27]. RF data were generated at a sampling frequency rate of 100 MHz and subsequently down-sampled to 40 MHz to match the rate of the Ultrasonix scanner. Sample US images reconstructed based on simulated RF data are presented in Fig. 2. RF data frames were divided into training, validation and test data with a 0.75/0.1/0.15 split. Next, the sliding window technique was used to divide each frame into 3 mm × 3 mm 2D patches (150 × 30 samples) to enable the development of temperature monitoring methods [8]. The total number of patches was equal to 72 000. Field II simulations were performed in Matlab (MathWorks, USA).

2.3. Scatterer density estimation

Small 2D patches of RF data were used to train a DenseNet CNN for the scatterer density prediction [28]. Dense convolutional networks connect each layer to every other layer in a feed-forward fashion. We selected DenseNet architecture for several reasons. First, dense connections alleviate the vanishing-gradient problem and encourage reuse of feature maps. Second, dense networks are commonly more compact and perform better than conventional CNNs, such as the VGG19 [28].

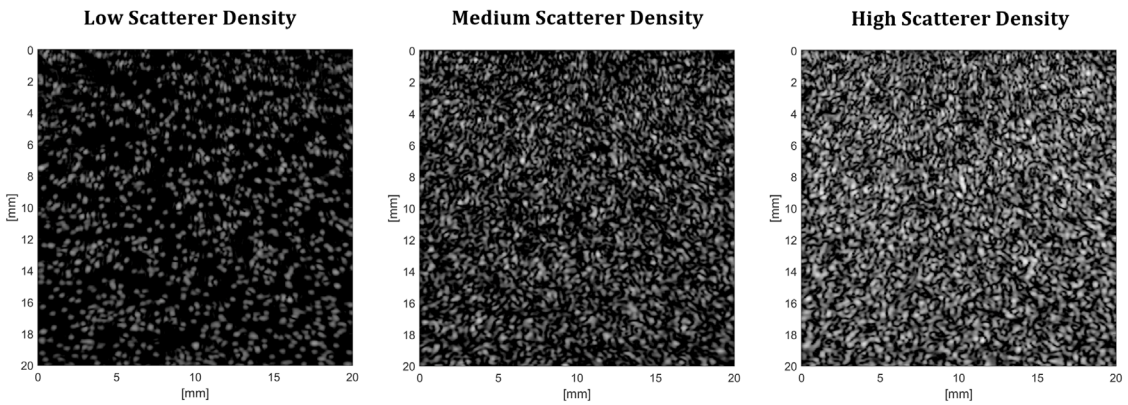

Fig. 2. Simulated US image presenting three different scattering scenarios. 2D patches of simulated RF data were used to pre-train Siamese network.

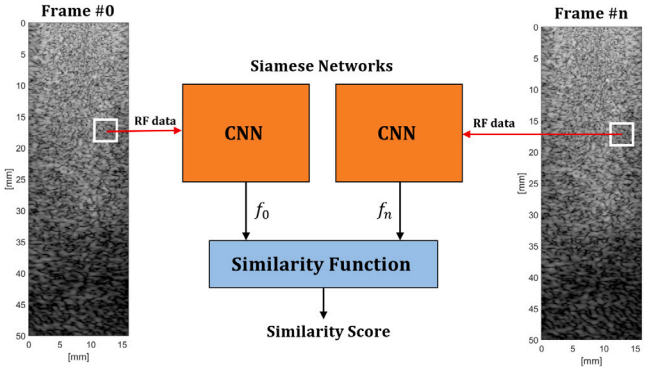

Fig. 3. Pipeline illustrating the proposed approach. Two identical networks (Siamese model) are used to extract feature vectors based on small 2D patches of RF data corresponding to different time points. Next, a similarity function is utilized to compare the feature vectors and yield a similarity score presenting local change in RF data characteristics.

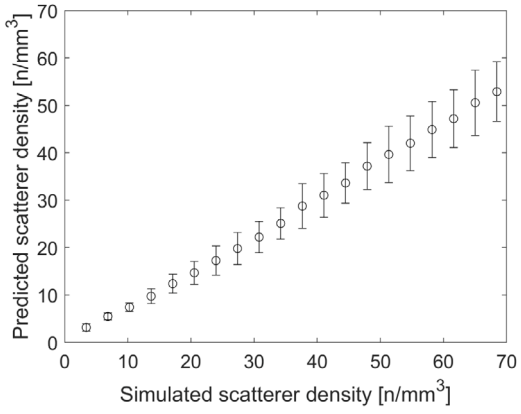

Fig. 4. Test results (means and standard deviations) achieved by the network trained to predict scatterer density.

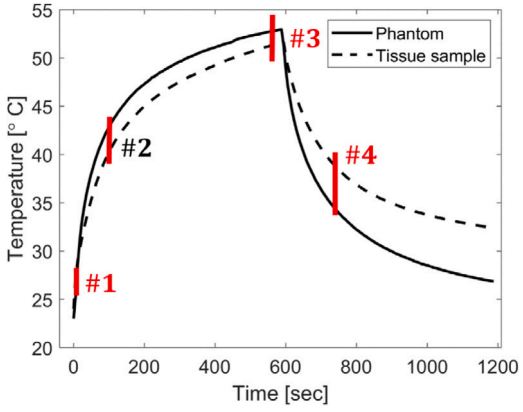

Fig. 5. Focal spot temperature distributions determined using thermocouple for the phantom and tissue sample. Four time points were selected to visualize the US images and parametric maps presenting temperature spatial distributions.

Our network included 4 dense blocks. Each block consisted of 8 layers composed of three subsequent operations: batch normalization (BN), rectified linear unit (ReLu) activation function and 3 × 3 convolutions. The growth rate of the dense network was set to 12. Each dense block was followed by a transition layer consisting of three subsequent operations: BN, 1 × 1 convolutions and 2 × 2 average pooling. The compression rate of the transition layers was set to 0.5, therefore each transition layer reduced the number of feature maps twice. After the last dense block, global average pooling was applied followed by a densely connected layer and ReLU activation function suitable for the scatterer density prediction. A detailed description of the DenseNet architecture can be found in the original paper [28].

Our network was trained using SGD optimizer with momentum to minimize the mean absolute error loss. Dropout regularization with a rate of 0.2 was applied to all weights of the network to improve the training. Learning rate and batch size were set to 0.01 and 128, respectively. During the training, we monitored the loss score on the validation set and terminated the training if no improvement was observed after 12 epochs. Following the training, we assessed the model using the test set to report the independent performance of the model. Neural models were developed using Python and TensorFlow library [29].

2.4. Siamese network

The Siamese model consisted of two identical networks described in the previous subsection. To compare the nth RF data frame with the frame corresponding to the start of the heating (frame #0), we applied the following procedure. First, we used the sliding window technique to extract 3 mm × 3 mm (150 × 30 samples) patches of RF data with an 80% overlap ratio. Second, patches corresponding to the same spatial location were used as input to the Siamese network. For each Siamese twin we extracted the neural features from the global average pooling layer. Next, the similarity between the extracted feature vectors was assessed using l_2 norm. To generate the parametric map $M(x, y, n)$ we

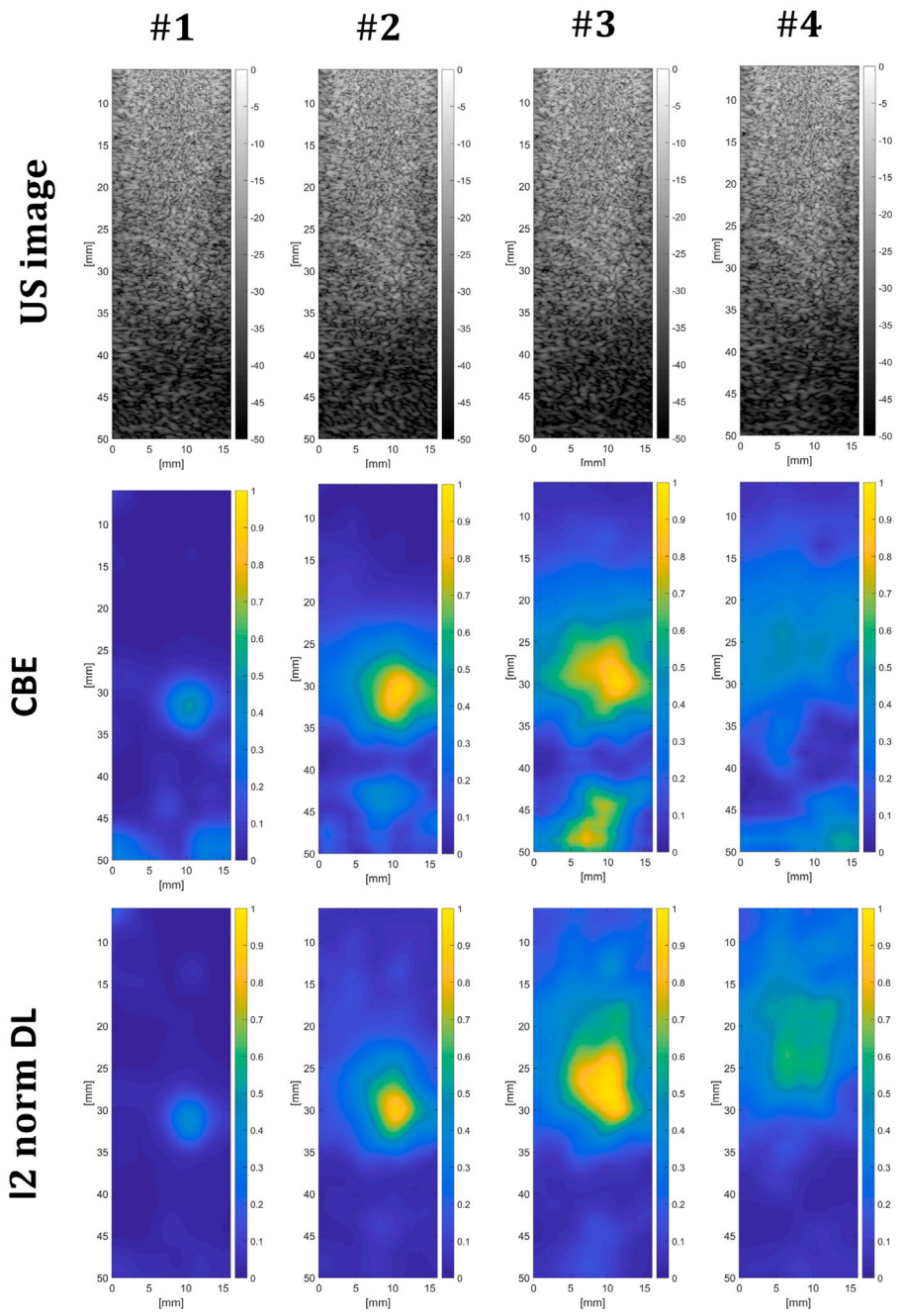

Fig. 6. Parametric maps presenting spatial distributions of the CBE and the l_2 norm DL based similarity score calculated for different time points for the experiment including tissue-mimicking phantom (see Fig. 5).

used the following equation:

$$M(x, y, n) = f(h(x, y, 0), h(x, y, n)), \tag{1}$$

where $h(x, y, n)$ denotes the feature vector corresponding to the nth frame at (x, y) spatial location, and $f(\cdot)$ stands for the l_2 norm similarity function. Pipeline of the proposed method is illustrated in Fig. 3. The similarity scores calculated for each patch were used to generate parametric maps presenting spatial differences in RF data between the frames. Given all maps, we normalized them to range from 0 to 1 based on the maximal similarity score found in the maps. Additionally, we assessed the temporal relationships between the similarity scores and the temperature distribution recorded by the closest thermocouple. For each parametric map a 2 mm × 2mm region of interest was placed on the center heating area to calculate the average similarity score. Moreover, to assess the results we also applied linear regression analysis between the average scores and the temperature distribution corresponding to the heating stage [8]. Additionally, we implemented the CBE technique for the comparison [6]. Envelope of the RF signals was calculated with the Hilbert transform. Exactly the same sliding window technique as in the case of the DL method was applied to determine the CBE values. For each 2D patch, we used the following equation for the calculations:

$$\mathrm{CBE}(x, y, n) = \left|10\log_{10}\left(\frac{\mathrm{E}[(e(x, y, n))]}{\mathrm{E}[(e(x, y, 0))]}\right)\right|, \tag{2}$$

where $\mathrm{E}[(e(x, y, n))]$ stands for the expected (average) envelope value of the 2D patch at position (x, y) for the nth RF data frame. Similarly, the CBE values were normalized to range from 0 to 1.

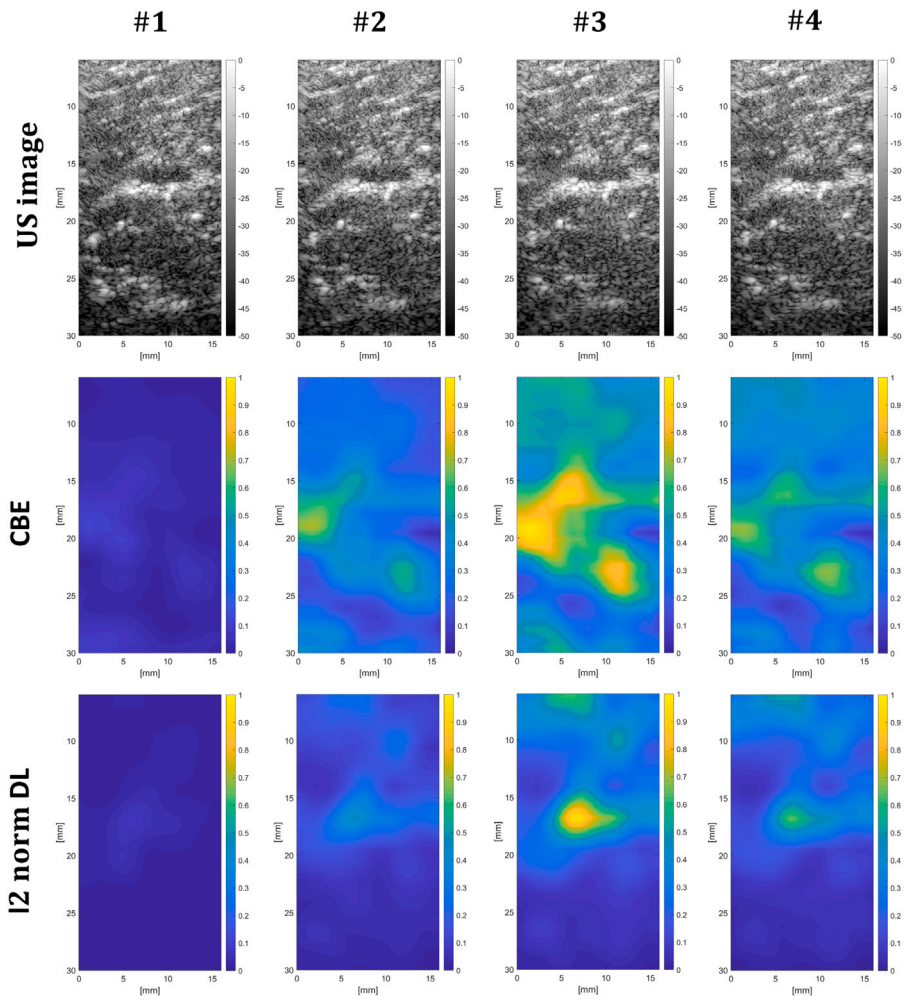

Fig. 7. Parametric maps presenting spatial distributions of the CBE and the l_2 norm DL based similarity score calculated for different time points for the experiment including *ex-vivo* tissue sample (see Fig. 5).

3. Results

3.1. Simulated data

Fig. 4 shows the relationship between the mean scatterer densities calculated using test examples. The network achieved good results, with the linear correlation coefficient of 0.95 determined based on all test samples. However, slight bias towards lower scatterer densities was observed.

3.2. Experiments

The temporal distributions of temperature determined by the thermocouples for the points of the maximum heating are presented in Fig. 5. Four time points were selected to generate the visualizations of the spatiotemporal temperature distributions. The CBE and DL based parametric maps calculated for the phantom and the tissue samples are presented in Figs. 6 and 7, respectively. Compared to US images, we can observe that the parametric maps better depicted the regions corresponding to the heating. DL based parametric maps calculated with the Siamese network provided more smooth and artifact free spatiotemporal temperature distributions. In the case of the phantom CBE maps, a typical tail artifact could be observed. A ripple pattern appeared under the heated region and was visible in all four CBE parametric maps, especially in the case of the tissue-mimicking phantom. In comparison, the parametric maps generated with the network were not corrupted by this artifact. Moreover, the CBE maps calculated for the *ex-vivo* tissue samples were more noisy and less clearly depicted the heating region. Additionally, Fig. 8 shows the axial and lateral distributions of the parameters for the moment of the maximum heating (point #3 in Fig. 5) generated for the parametric image lines crossing the point of the maximal heating. Here, Fig. 8 presenting the axial parameter distribution clearly depicts the ripple artifact in the case of the CBE technique and the tissue-mimicking phantom.

A 2 mm × 2 mm ROI was placed on the max heating spot to calculate the local mean of each parametric map for each sample. Results presented in Fig. 9 show that the temporal score distributions were similar to the thermocouple measurements for both techniques (Fig. 5). However, slightly worse results were obtained for the experiment with the tissue sample. Fig. 10 presents regression results obtained for the heating phase for the CBE and DL score. In this case, we achieved good results for the tissue-mimicking phantom, with R^2 parameters equal to 0.97 for both methods. Results obtained for the tissue samples were worse, with R^2 parameters equal to 0.95 and 0.90 for the CBE and DL techniques, respectively.

4. Discussion

In this preliminary study, we proposed an unsupervised DL based approach to temperature monitoring in US imaging. Results presented that the proposed method might serve as a good approach to the HIFU heating spot localization. Our study addressed several important

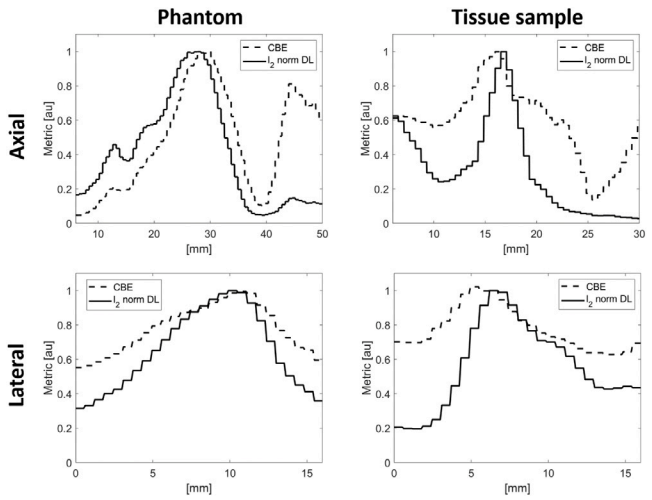

Fig. 8. Axial and lateral distributions of the CBE parameter and the l_2 norm based DL score calculated for the phantom and tissue sample for the moment of the maximum heating (see #3 in Figs. 5 and 6).

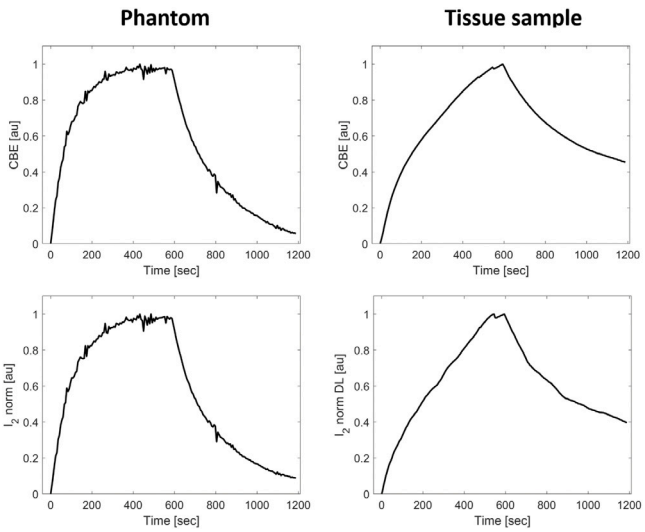

Fig. 9. CBE and l_2 norm DL method based similarity scores calculated for the center heating areas of the phantom and tissue sample.

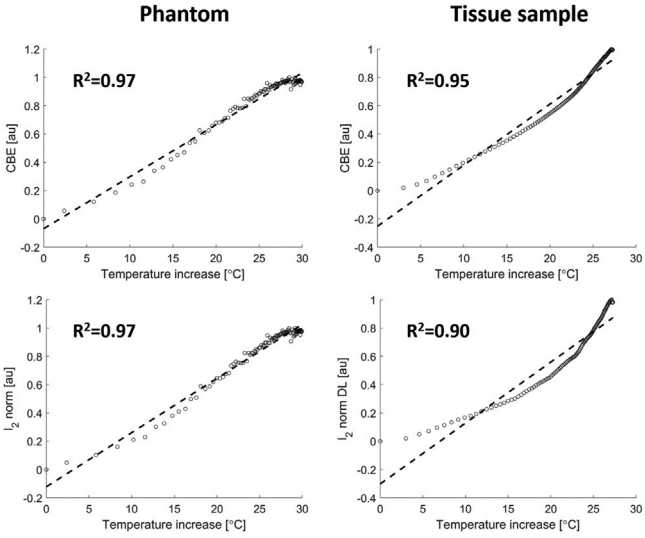

Fig. 10. Linear regression results obtained for the CBE and the l_2 norm DL method calculated for the center heating areas of the phantom and the tissue sample.

problems. In comparison to standard US images, it is usually more difficult to collect large volumes of RF data. For example, acquisition of RF data requires a research US scanner. In the case of the experiments related to temperature monitoring, acquisition of RF data is also time-consuming and expensive. In this work, we pre-trained a neural network using simulated RF data. Field II software was utilized to generate large volumes of RF data presenting different scattering properties. Next, the network pre-trained on simulated data was successfully used for temperature monitoring based on real RF data. We used the Siamese twin network to generate spatiotemporal maps illustrating distribution of temperature during the experiments. In comparison to the previously proposed DL techniques for temperature monitoring, our approach was generic and operated in an unsupervised manner [20,21]. The Siamese network was used in a non-parametric way to compare small 2D patches of RF data. The proposed method did not depend on a specific physical model of the tissue. While in this work we presented the usefulness of our approach based on a HIFU heating experiment, the proposed method is general and can be potentially used for various conditions and tissues. The proposed DL method provided similar monitoring results to the CBE parameter for the region of the maximal heating (Fig. 9). The CBE parameter has been widely used for the temperature monitoring and is considered to be among the better performing monitoring techniques [3]. However, the CBE imaging is commonly associated with the ripple artifact, which occurs under the heating region due to the local change of the sound speed in the heated region [30,31]. This local change causes the time shift of the RF signals under the heating region and affects CBE calculations, which are based on the average RF signal envelope samples. Compared to the CBE imaging, the DL method did not generate the ripple artifacts, which could be due to the fact that the network was trained to predict tissue backscatter properties. Therefore, the DL score was not as sensitive as the CBE to the RF signal time shift issue. Moreover, in the case of the *ex-vivo* tissue sample experiments, our approach provided parametric maps that better illustrated the spatial temperature distribution.

There are several issues related to our method. First of all, we used thermocouples as the reference, which makes the assessment of the results difficult. Temperature distribution presented in Fig. 5 is only related to one spatial location within each sample. To better assess the spatial distribution of temperature, it would be necessary to use magnetic resonance imaging [32,33]. Nevertheless, Figs. 9 and 10 show that our results were in a good agreement with thermocouple measurements. Second, more experiments are necessary to better validate the proposed method. In our case, we used a single HIFU transducer for the heating. Third, the proposed DL based approach lacks interpretability compared to the CBE or QUS techniques, which utilize well-known tissue physical properties for tissue characterization. This is a common issue related to neural networks, which are considered as black-box models. In our case, the Siamese twin network was pre-trained to predict scatterer density based on simulated RF data, which may be related to the backscatter coefficient or the number of scatterers per resolution cell of the Homodyned K distribution. However, in our Field II simulations, we did not modify other tissue properties, such as the attenuation coefficient. We also did not simulate tissue interfaces or strong coherent reflections, typically present in regular US images. This issue may explain the worse performance of our method in the case of the *ex-vivo* tissue sample experiment. Pre-training on more diverse simulated RF data could perhaps lead to better results in this case. In future, we would like to investigate the usefulness of other types of RF data for network pre-training. It would also interesting to utilize more sophisticated RF data simulators, such as the K-wave software [34]. Fourth, in our experiment the samples were static, we did not have

to perform motion correction, which would be probably necessary in clinical practice due to patient and tissue motion.

5. Conclusions

In this work, we presented a deep learning method for tissue temperature monitoring in focused ultrasound treatment. We used Siamese networks to locally compare small 2D patches of RF data to yield similarity scores enabling assessment of tissue temperature. The proposed method worked in an unsupervised manner and did not require training. Our future work will benefit from a larger number of experiments and the investigation of different deep learning based approaches.

Declaration of competing interest

The authors declare that they have no known competing financial interests or personal relationships that could have appeared to influence the work reported in this paper.

Acknowledgment

This work was supported by the National Science Center of Poland (grant number 2011/03/B/ST7/03347).

References

[1] J. Foiret, K.W. Ferrara, Spatial and temporal control of hyperthermia using real time ultrasonic thermal strain imaging with motion compensation, phantom study, PLoS One 10 (8) (2015) e0134938.
[2] J.E. Kennedy, High-intensity focused ultrasound in the treatment of solid tumours, Nature Rev. Cancer 5 (4) (2005) 321–327.
[3] M.A. Lewis, R.M. Staruch, R. Chopra, Thermometry and ablation monitoring with ultrasound, Int. J. Hyperthermia 31 (2) (2015) 163–181.
[4] M.L. Oelze, J. Mamou, Review of quantitative ultrasound: Envelope statistics and backscatter coefficient imaging and contributions to diagnostic ultrasound, IEEE Trans. Ultrason. Ferroelectr. Freq. Control 63 (2) (2016) 336–351.
[5] P.M. Shankar, Ultrasonic tissue characterization using a generalized Nakagami model, IEEE Trans. Ultrason. Ferroelectr. Freq. Control 48 (6) (2001) 1716–1720.
[6] J.W. Trobaugh, R.M. Arthur, W.L. Straube, E.G. Moros, A simulation model for ultrasonic temperature imaging using change in backscattered energy, Ultrasound Med. Biol. 34 (2) (2008) 289–298.
[7] X. Li, G. Ghoshal, R.J. Lavarello, M.L. Oelze, Exploring potential mechanisms responsible for observed changes of ultrasonic backscattered energy with temperature variations, Med. Phys. 41 (5) (2014) 052901.
[8] K. Yang, Q. Li, H.-L. Liu, C.-K. Chen, C.-W. Huang, J.-R. Chen, Y.-W. Tsai, Z. Zhou, P.-H. Tsui, Frequency-domain CBE imaging for ultrasound localization of the HIFU focal spot: a feasibility study, Sci. Rep. 10 (1) (2020) 1–10.
[9] P.-H. Tsui, Y.-C. Shu, W.-S. Chen, H.-L. Liu, I.-T. Hsiao, Y.-T. Chien, Ultrasound temperature estimation based on probability variation of backscatter data, Med. Phys. 39 (5) (2012) 2369–2385.
[10] B. Gambin, E. Kruglenko, Temperature measurement by statistical parameters of ultrasound signal backscattered from tissue samples., Acta Phys. Pol. A 128 (2015).
[11] M. Byra, E. Kruglenko, B. Gambin, A. Nowicki, Temperature monitoring during focused ultrasound treatment by means of the homodyned k distribution, Acta Phys. Polon. A (2013).
[12] S. Song, P.-H. Tsui, W. Wu, S. Wu, Z. Zhou, Monitoring microwave ablation using ultrasound homodyned k imaging based on the noise-assisted correlation algorithm: An ex vivo study, Ultrasonics 110 (2021) 106287.
[13] C.H. Seo, Y. Shi, S.-W. Huang, K. Kim, M. O'Donnell, Thermal strain imaging: a review, Interface Focus 1 (4) (2011) 649–664.
[14] B. Arnal, M. Pernot, M. Tanter, Monitoring of thermal therapy based on shear modulus changes: II. Shear wave imaging of thermal lesions, IEEE Trans. Ultrason. Ferroelectr. Freq. Control 58 (8) (2011) 1603–1611.
[15] R. Righetti, F. Kallel, R.J. Stafford, R.E. Price, T.A. Krouskop, J.D. Hazle, J. Ophir, Elastographic characterization of HIFU-induced lesions in canine livers, Ultrasound Med. Biol. 25 (7) (1999) 1099–1113.
[16] G. Litjens, T. Kooi, B.E. Bejnordi, A.A.A. Setio, F. Ciompi, M. Ghafoorian, J.A. Van Der Laak, B. Van Ginneken, C.I. Sánchez, A survey on deep learning in medical image analysis, Med. Image Anal. 42 (2017) 60–88.
[17] J. Kim, H.J. Kim, C. Kim, W.H. Kim, Artificial intelligence in breast ultrasonography, Ultrasonography 40 (2) (2021) 183.
[18] Y. Kim, C. Audigier, E.M. Anas, J. Ziegle, M. Friebe, E.M. Boctor, CUSt: CNN for ultrasound thermal image reconstruction using sparse time-of-flight information, in: Simulation, Image Processing, and Ultrasound Systems for Assisted Diagnosis and Navigation, Springer, 2018, pp. 29–37.
[19] Y. Kim, C. Audigier, N. Ellens, E.M. Boctor, Low-cost ultrasound thermometry for HIFU therapy using CNN, in: 2018 IEEE International Ultrasonics Symposium (IUS), IEEE, 2018, pp. 1–9.
[20] C. Chen, Y. Kim, C. Audigier, E.M. Boctor, Ultrasound thermometry using an ultrasound element and deep learning for HIFU, in: 2019 IEEE International Ultrasonics Symposium (IUS), IEEE, 2019, pp. 548–551.
[21] S. Zhang, S. Wu, S. Shang, X. Qin, X. Jia, D. Li, Z. Cui, T. Xu, G. Niu, A. Bouakaz, et al., Detection and monitoring of thermal lesions induced by microwave ablation using ultrasound imaging and convolutional neural networks, IEEE J. Biomed. Health Inform. 24 (4) (2019) 965–973.
[22] Y. Taigman, M. Yang, M. Ranzato, L. Wolf, Deepface: Closing the gap to human-level performance in face verification, in: Proceedings of the IEEE Conference on Computer Vision and Pattern Recognition, 2014, pp. 1701–1708.
[23] L. Bertinetto, J. Valmadre, J.F. Henriques, A. Vedaldi, P.H. Torr, Fully-convolutional siamese networks for object tracking, in: European Conference on Computer Vision, Springer, 2016, pp. 850–865.
[24] E. Kruglenko, B. Gambin, L. Cieślik, Soft tissue-mimicking materials with various number of scatterers and their acoustical characteristics, Hydroacoustics 16 (2013).
[25] J.A. Jensen, Field: A program for simulating ultrasound systems, in: 10th Nordicbaltic Conference on Biomedical Imaging, Vol. 4, Supplement 1, Part 1: 351–353, Citeseer, 1996.
[26] J.A. Jensen, N.B. Svendsen, Calculation of pressure fields from arbitrarily shaped, apodized, and excited ultrasound transducers, IEEE Trans. Ultrason. Ferroelectr. Freq. Control 39 (2) (1992) 262–267.
[27] X. Yu, Y. Guo, S.-M. Huang, M.-L. Li, W.-N. Lee, Beamforming effects on generalized Nakagami imaging, Phys. Med. Biol. 60 (19) (2015) 7513.
[28] G. Huang, Z. Liu, L. Van Der Maaten, K.Q. Weinberger, Densely connected convolutional networks, in: Proceedings of the IEEE Conference on Computer Vision and Pattern Recognition, 2017, pp. 4700–4708.
[29] M. Abadi, P. Barham, J. Chen, Z. Chen, A. Davis, J. Dean, M. Devin, S. Ghemawat, G. Irving, M. Isard, et al., Tensorflow: A system for large-scale machine learning, in: 12th {USENIX} Symposium on Operating Systems Design and Implementation ({OSDI} 16), 2016, pp. 265–283.
[30] K. Choi, D. Kong, J. Park, J. Cho, H.-K. Lee, Noninvasive ultrasound temperature imaging with fusion algorithm, in: 2012 IEEE International Ultrasonics Symposium, IEEE, 2012, pp. 933–936.
[31] C. Simon, P. VanBaren, E.S. Ebbini, Two-dimensional temperature estimation using diagnostic ultrasound, IEEE Trans. Ultrason. Ferroelectr. Freq. Control 45 (4) (1998) 1088–1099.
[32] S. Li, P.-H. Wu, Magnetic resonance image-guided versus ultrasound-guided high-intensity focused ultrasound in the treatment of breast cancer, Chinese J. Cancer 32 (8) (2013) 441.
[33] T. Kujawska, W. Secomski, M. Byra, M. Postema, A. Nowicki, Annular phased array transducer for preclinical testing of anti-cancer drug efficacy on small animals, Ultrasonics 76 (2017) 92–98.
[34] B.E. Treeby, B.T. Cox, K-Wave: MATLAB toolbox for the simulation and reconstruction of photoacoustic wave fields, J. Biomed. Optics 15 (2) (2010) 021314.